Environmental Science and Pollution Research (2024) 31:44759–44769
https://doi.org/10.1007/s11356-024-34191-z

RESEARCH ARTICLE

Fabrication of versatile Fe_3O_4/GO/Au composite nanomaterial as SERS-active substrate for detection of pesticide residue

Rui Wu[1] · **Xi Song**[1] · **Guanghui Tian**[1]

Received: 17 February 2024 / Accepted: 26 June 2024 / Published online: 2 July 2024

Abstract

Highly active Fe_3O_4/GO/Au composite nanomaterial was fabricated as a substrate of surface-enhanced Raman spectroscopy (SERS) and applied for pesticide residue detection. The three-layer multifunctional Fe_3O_4/GO/Au nanoparticles (NPs) were designed by facile method, with high hotspots, and were characterized by various techniques, including ultraviolet spectrophotometry (UV), X-ray diffraction (XRD), infrared absorption spectrometer (IR), and transmission electron microscopy (TEM). The performance of Fe_3O_4/GO/Au was evaluated by Raman spectroscopy with R6G as a probe molecule to verify its enhancement effect. It exhibited a strong Raman signal with 10^{-6} M of R6G. Furthermore, the presence of Fe_3O_4/GO/Au nanohybrid enabled the SERS-based method to detect mancozeb and showed an excellent linear relationship in the range of 0.25–25 ppm, with a low limit of detection (0.077 ppm), satisfactory EF, stability, and repeatability. In addition, the mechanism of SERS enhancement with electromagnetic mechanism (EM) and chemical mechanism (CM) was discussed in detail. Therefore, the proposed SERS approach holds promise as an auxiliary technique for screening contaminated agricultural products, environmental sample, and food in the future.

Keywords SERS · Substrate · Fe_3O_4/GO/Au · Composite nanomaterial · Pesticide residue detection · mancozeb

Introduction

Food is the basic necessity for people's survival. With the rapid development of the economy, food and environmental pollution are major issues related to national health and safety. Nowadays, more and more harmful chemicals are entering the environment of human living (Ye et al. 2017; Ji et al. 2023). As a contact fungicide, dithiocarbamate compound (DTC) is effective against pathogens and widely used for crops, such as vegetables and fruits. However, with the introduction of such pesticides into the environment, their physical, chemical, and biological processes can be transformed into harmful substances and cause disease (Wang et al. 2020). As a common dithiocarbamate insecticide, the metabolite of mancozeb is ethylene thiourea (ETU), which has been classified as a category III carcinogen by the International Agency for Research on Cancer. Long-term consumption of ETU can cause adverse effects such as embryonic malformations and thyroid abnormalities (Dall'Agnol et al. 2021). Therefore, it should be of great significance to develop a fast, sensitive, accurate, and effective method to analyze and detect low-concentration fungicides contained in the environment and food.

In recent years, it has witnessed the great progress in pesticide residue detection technology which leads to the proposal of various technical approaches for detecting pesticide residue in fruits and vegetables (Łozowicka et al. 2017). These methods include gas chromatography-mass spectrometry (Wang et al. 2022), liquid chromatography-mass spectrometry (Yang et al. 2022), immunoassay (Xu et al. 2022a, b), and SERS. SERS is a rapid detection technique that has been utilized for food identification, quantitative analysis, and classification of food pollutants. SERS is well known for its sensitivity and ability to quickly recognize fingerprints, making it a valuable analytical tool for both qualitative and quantitative detection of food samples (Weng et al. 2019; Han et al. 2021; Zhou et al. 2021; Yang et al. 2023). SERS was first discovered in 1974, its principle is to amplify the

Responsible Editor: Angeles Blanco

✉ Rui Wu
wurui@snut.edu.cn; hftffc@163.com

[1] Shaanxi Key Laboratory of Catalysis, College of Chemical and Environment Science, Shaanxi University of Technology, Hanzhong 723001, Shaanxi, China

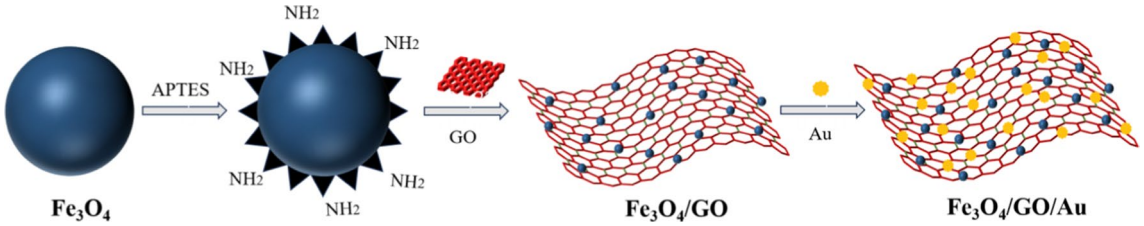

Scheme 1 Schematic illustration of the fabrication of Fe_3O_4/GO/Au NPs

Raman signals of molecules close to the surface of metal nanostructures as SERS substrate through the electromagnetic enhancement effect and chemical enhancement mechanism of noble metal nanostructures. In other words, the SERS substrate relies on plasmonic nanostructures, particularly Au and Ag NPs with strong surface plasmon resonance (SPR) effect (Atanasov et al 2019a, b). The performance of SERS can be adjusted by changing the size, morphology, and composition of the nanomaterials (Dick et al. 2016; Bi et al. 2023; Ye et al. 2020; Van Vu et al. 2023; Ying et al. 2023). Because of the development of nanotechnology, the SERS detection technique has entered a new stage of rapid progress. For instance, Wu et al.developed a SERS active substrate based on Au nanorods, which is applied to lakes and various fruits contaminated with methyl parathion (Wu et al. 2019). Deng demonstrated a SERS sensor covered by Ag nanowire network. The wrinkled biomimetic Ag as SERS substrate, with high density of hotspots, exhibited strong SERS effect and enabled the detection of pesticide molecules (Deng et al. 2023). Single plasmonic metal as SERS substrate with finite property cannot completely meet the requirements of analysis, such as weak affinity between analyte and substrate and low sensitivity of SERS. Versatile substrate with exceptional performance is crucial for practical applications. To address this, it is necessary to develop a SERS composite substrate that combines capture ability, rapid enrichment ability, ease of separation, and plasma resonance effect. Compared with ordinary nanoparticles, magnetic nanocomposites can achieve efficient enrichment for the target material and rapid separation by an external magnetic field (Zheng et al. 2021; Tiryaki et al. 2024). Notably, the combination of magnetic-plasmonic nanocomposites can achieve significant enhancements in the SERS performance.

In recent years, graphene oxide (GO) has gained attention in various fields due to its unique physical and chemical properties, especially the large specific surface area. Its large specific surface area and conjugated structure contribute to its fast adsorption rate for aromatic ring organic pollutants. In addition, GO and other semiconductor nanomaterials, such as TiO_2, ZnO, MoS_2, CuO, Fe_2O_3, Cu_2O, Cu_2S, Cu_2Se, CuTe, CdS, PbS, AgS, CdTe, and NiO, demonstrate high SERS activity, and they contribute to the chemical enhancements (Sakano et al 2008; Shukla et al 2023; Avadaiappan et al 2022; Liu et al 2024; Fu et al 2024; Zheng et al 2023). The introduction of GO not only overcomes some inherent defects of SERS, but also has an excellent synergistic effect with traditional precious metal NPs as substrate (Weis et al. 2018, Suzuki 2019, Meenakshi et al. 2023). These characteristics of GO not only provide advantages for the preparation of composite substrate materials, but also expand the application field of SERS to a certain extent.

In order to achieve rapid and sensitive detection of pesticide residues in food, a three-layer multi-functional SERS composite substrate (Fe_3O_4/GO/Au) was designed and constructed, as depicted in Scheme 1. Combining the advantage of each layer, the prepared composite substrate for SERS analysis can achieve rapid separation and enrichment of target molecules without requiring excessive pre-treatment time, and the substrate provides abundant hotspots and amplifies the signal through synergy. Due to the excellent properties of Fe_3O_4/GO/Au above, mancozeb was directly detected. To verify the feasibility of the method, mancozeb in pakchoi was tested, and successful detection with high sensitivity and recovery rate was achieved. The novel composite nanomaterial substrate paves the way for the detection of pesticide residues and opens a new path for analysis in the food, environment, and biomedicine field.

Material and methods

Chemicals and materials

Chloroauric acid, ferric chloride, ferrous sulfate, graphite powder (industrial grade), potassium permanganate, trisodium citrate, and ascorbic acid were purchased from Aladdin Reagent (Shanghai) Co., Ltd. (Shanghai, China). Concentrated sulfuric acid, isopropanol, polyvinylimide, sodium nitrate, and sodium chloride were obtained from Sinopharm Chemical Reagent Co., Ltd. (Beijing, China). All glassware and stirring bars were soaked in aqua regia for 24 h and rinsed several times with ultrapure water before use. All chemicals were used without further purification.

Milli-Q ultrapure water was used for all solution preparations in the study.

Preparation of the materials for SERS substrate

Preparation of Fe_3O_4 particles

Co-precipitation method was employed to synthesize Fe_3O_4 NPs. Initially, 80 mL of deionized water was added to 250 mL of three-neck flask and stirred mechanically. To remove oxygen, nitrogen flowed through the solution. Subsequently, 0.8641 g of ferrous sulfate and 0.4448 g of ferric chloride were added to the flask and completely dissolved quickly. The solution exhibited an orange-yellow. The temperature of the solution was then raised to 60 °C, and the pH of the solution was adjusted to 9.0–10.0 by ammonia. The solution rapidly changed from orange to black. After 30 min, the temperature was increased to 85 °C, and the mixture was aged for 30 min under the protection of nitrogen. Then, the three-neck flask was removed and allowed to cool to room temperature. The Fe_3O_4 solution was transferred to the beaker, and the Fe_3O_4 NPs were separated from the solution by the external magnetic field. The separated Fe_3O_4 NPs were washed alternatively with deionized water and absolute ethanol several times. Finally, they were dried at 50 °C in the oven to obtain magnetic Fe_3O_4 NPs (Jinzi and Chunyan 2020).

Preparation of graphene oxide

GO was obtained using a modified Hummers method (Lin et al. 2021). Initially, 40.0 mL of concentrated sulfuric acid was measured and mixed with 1.0 g of graphite powder and 0.5 g of sodium nitrate. The mixture was mechanically stirred for 30 min in an ice-water bath. Subsequently, 5.0 g of potassium permanganate was added gradually in ten small portions, and the reaction was continued for 60 min. The resulting mixture was then transferred to the water bath, kept temperature at 35 °C, and stirred continuously for 60 min. Then, 50 mL of deionized water was slowly added, and the temperature was adjusted to 80 °C; the reaction was carried out for 30 min. Finally, 100 mL of deionized water and 30% hydrogen peroxide were rapidly added until no bubbles were generated, resulting in an earthy yellow product. Once the reaction is complete, the obtained product is dried in a vacuum drying oven at 35 °C and labeled for future use.

Preparation of Fe_3O_4/GO

A total of 0.5 g of dried Fe_3O_4 NPs was added into 25 mL of isopropyl alcohol and dissolved by ultrasonic waves for 40 min. A total of 0.15 mL of (3-aminopropyl)triethoxysilane (APTES) was added gradually drop by drop, followed by ultrasonic treatment for 10 min (Akamine et al. 2021). Then, the mixture was transferred to the flask and kept at 85 °C with reflux for 3 h. After cooling to room temperature, the product was washed alternately with ethanol and deionized water and separated the amino-modified Fe_3O_4 by using a magnet. The obtained product was added to 35 mL of deionized water and dispersed completely. Similarly, 0.15 g of graphene oxide was dissolved in 35 mL of deionized water to obtain graphene oxide solution. The obtained solution was mixed and sonicated for 30 min. Stir the mixture overnight at room temperature, then magnetically separate it, and wash it several times with ethanol and deionized water alternately. Finally, dry it under vacuum at 60 °C, label it, and set it aside.

Preparation of Au NPS

To prepare the Au seeds, first, 0.5 mL of $HAuCl_4$ (1%) was added to 30 mL of deionized water and stirred at room temperature for 10 min. Then, 0.2 mL of sodium citrate (1%) solution was added and continued for about 5 min with stirring. Followed by the addition of 1 mL of $NaBH_4$ (0.375%) solution, and stirring for 10 min, orange-red Au seeds appeared. Next, 50 mL of deionized water in a conical flask was accurately measured. 0.35 mL of $HAuCl_4$ (1%), and 0.35 mL of Au seeds were added and stirred for 5 min to create a homogeneous mixture at room temperature. Then, 0.1mL of sodium citrate (1%) solution and 0.1mL of polyvinylpyrrolidone (1%wt) were added, followed by stirring for 3 min. The temperature was then raised to 45 °C. After stirring for an additional 5 min, 0.5 mL of ascorbic acid (0.3 M) solution was added dropwise, and blue-violet Au sol was obtained (Wu et al. 2019).

Preparation of Fe_3O_4/GO/Au

Initially, 200 mg of Fe_3O_4/GO was added to 100 mL of deionized water, and 1 mL of polyethyleneimine in 49 mL of deionized water was added. The solution was mixed under ultrasonication for 40 min at room temperature to ensure complete dispersion, followed by mechanical stirring. After 24 h, magnetic separation was performed, followed by alternating washes with deionized water and ethanol for 3–4 times. The product was then dried. Next, 100 mg of amino-functionalized Fe_3O_4/GO was accurately weighed and dispersed in 25 mL of deionized water with ultrasonication. Then, 20 mL of Au sol was added, followed by ultrasonication for 15 min. The obtained Fe_3O_4/GO/Au was dried in the oven at 60 °C (Ghanei and Hosseinifar 2020).

Characterization

The X-ray diffraction (XRD) data was recorded on the D8ADVANCE diffractometer, with Cu as the target source, and scanned in the 2θ range of 10 ~ 80°. The UV–visible absorption peak and the infrared characteristic peak of the prepared material were measured, respectively. The structure and morphology of synthesized Fe_3O_4/GO/Au nanoparticles were studied by transmission electron microscopy (TEM). Raman spectra were obtained using a confocal microscopy Raman spectrometer system (Horiba, LabRAMHR) with an excitation wavelength of 785 nm. The laser power and integration time are set to 20 mW and 12 s, respectively. Twenty microliters of the Fe_3O_4/GO/Au aqueous suspension mixed with 20 µL of R6G, respectively, and sonicated for 30 min. R6G was detected by using 785 nm laser.

Application of active substrates

Detection of mancozeb with standard solution

A stock solution of mancozeb was prepared in pyridine at a concentration of 100 ppm. This stock solution was then diluted with deionized water to obtain a series of mancozeb concentrations (0.5 ppm, 1 ppm, 10 ppm, 25 ppm, and 50 ppm) as the working standard solution. Prior to SERS measurement, 1 mL of the mancozeb standard solution with different concentrations was added to 5 mL of centrifuge tube containing 3 mL of Fe_3O_4/GO/Au. One hundred microliters of sodium chloride solution was added and sonicated. Thirty microliters of a portion of the resulting solution was analyzed using laser confocal microscopy and Raman spectroscopy (Atanasov et al. 2019a, b). For SERS measurements, a 785 nm laser was employed as an excitation source, with an acquisition time of 12 s and a laser power of 20 mW. Spectra were collected in the range of 400–1600 cm^{-1}.

Detection of mancozeb in real sample

Fresh pakchoi was purchased from the local supermarket and was used as tested samples. The QuEchERS (quick, easy, cheap, effective, rugged, and safe) method was followed to extract mancozeb from fresh pakchoi (Pan et al. 2021). Specifically, the purchased pakchoi was washed and dried, and 10 g of the sample was weighed into a 50 mL centrifuge tube. Then, 5 mL of acetonitrile, 1g of sodium chloride, and 0.2 g of anhydrous sodium acetate were added sequentially. The tube was shaken well and vortexed, followed by centrifugation at 4200 rpm for 5 min. The supernatant of the pakchoi appeared green. Two milliliters of the supernatant was transferred to a 10 mL centrifuge tube containing an appropriate amount of anhydrous magnesium sulfate and graphitized carbon black which were used to primarily remove the influence of chlorophyll and vitamins in the pakchoi. The solution was centrifuged for 5 min to obtain a colorless supernatant. The suspension was filtered and used for SERS measurements. In order to illustrate the feasibility of the method, a spiked recovery experiment was performed. The spiked solution with different concentrations was added into the unprocessed pakchoi. The QuEchERS method was used to extract mancozeb from pakchoi for SERS measurement. The detection procedure was the same as for the standard solution determination.

The test of activity, stability, and repeatability of Fe_3O_4/GO/Au

In order to quantify the SERS ability, the analytical enhancement factor (EF) was estimated. The formulation (LOD = 3δ/k) was used to determine the limit of detection (LOD). To examine the stability of Fe_3O_4/GO/Au, time-dependent SERS measurements were performed. To assess the repeatability of Fe_3O_4/GO/Au, three samples were obtained following the same conditions, at 11 random locations on the substrate.

Results and discussion

Characterization of Fe_3O_4/GO/Au nanocomposites

The crystal structures of Fe_3O_4, GO, and Fe_3O_4/GO/Au NPs were characterized by XRD, and the results were displayed in Fig. 1. The XRD spectrum of Fe_3O_4 showed strong diffraction peaks with 2θ at 30.2°, 35.6°, 43.2°, 57.1°, and 62.7°, corresponding to 220, 311, 400, 511, and 440, respectively, consistent with the spinel structure of Fe_3O_4 (JCPDS No.19–0629) (He et al. 2022). It was indicated that the prepared sample is pure Fe_3O_4. A new sharp peak

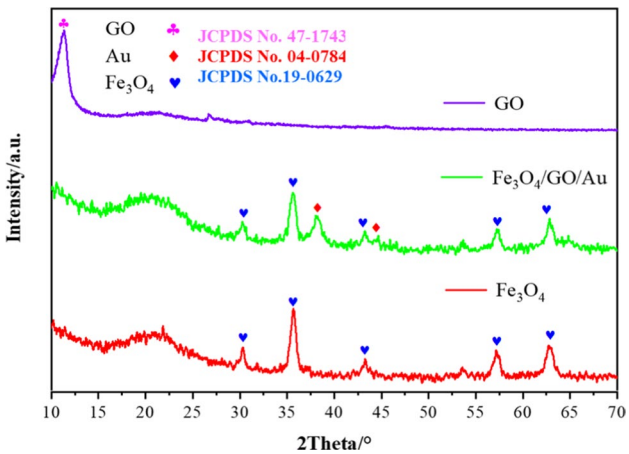

Fig. 1 XRD of the GO, Fe_3O_4, and Fe_3O_4/GO/Au

appears at 11.3°, which belongs to the peak of GO (JCPDS No.47–1743) (Supriyanto et al. 2018). In addition, there is a clear diffraction peak at 26.6°, which may be due to insufficient oxidation time resulting in incomplete oxidation of graphite. In the Fe_3O_4/GO/Au spectrum, there are two main diffraction peaks with 2θ at 38.0° and 44.6°, which correspond to the (111) and (200) crystal planes of Au (JCPDS No. 04–0784) (Wu et al. 2023), respectively. Except for the diffraction peaks of Fe_3O_4, Au, and GO, no other diffraction peaks were found. This may be due to the destruction of oxygen-containing functional groups on the surface of oxidized graphene. In a word, three-layer multifunctional Fe_3O_4/GO/Au composite materials were successfully fabricated.

The Fe_3O_4/GO/Au composite materials were identified by infrared spectra, ranging from 500 to 4000 cm^{-1}, as shown in Fig. 2. The IR spectra of GO showed peaks at 1721, 1632, 1395, and 1042 cm^{-1}, indicating the presence of hydrophilic functional groups such as C = O and C–O–C on the surface or edge of the prepared GO. It not only facilitates the stable existence of the composite material in water, but also enriches the analyte. In the IR spectrum of Fe_3O_4/GO/Au composite material, the stretching vibration of −C = O in the amide bond (−CONH) is at 1628 cm^{-1}, and the stretching vibration peak of C-N bond in the amide bond (−CONH) is at 1403 cm^{-1}. In addition, the absorption peak at 596cm^{-1} can be attributed to the stretching vibration peak of Fe–O, indicating the successful loading of Fe_3O_4 nanoparticles on GO (Khan et al. 2022).

Au, GO, and Fe_3O_4/GO/Au NPs were confirmed by UV. From Fig. 3, it can be seen that GO exhibits a distinct characteristic absorption peak at 230 nm, corresponding to the π → π transition of conjugated C = C on GO, indicating the successful preparation of graphene oxide using the Hummers method. The Au sol exhibits a significant absorption peak at around 523 nm (Jing et al. 2016). Compared with the

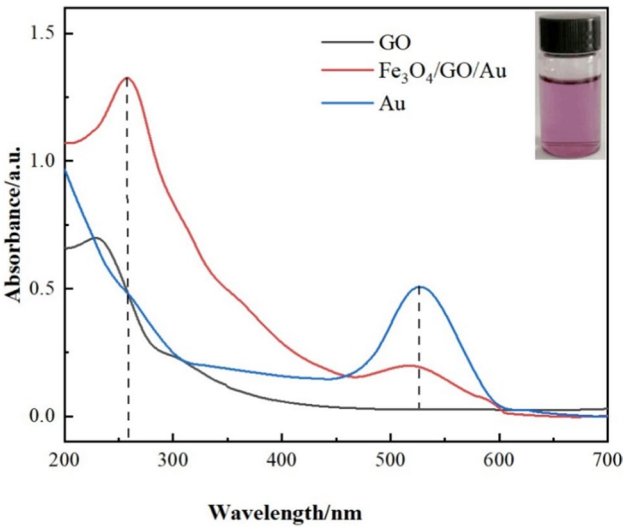

Fig. 3 Ultraviolet–visible absorption spectra of the GO, Fe_3O_4, and Fe_3O_4/GO/Au

obtained GO, the absorption peak of GO in Fe_3O_4/GO/Au showed a slight red shift. Maybe aggregation has occurred after interaction for the whole substrate. The Au of UV in Fe_3O_4/GO/Au was a little blue shift. The blue shift of 523 can be attributed to the localization of Au NPs on GO net (substrate), preventing Au NPs aggregation. This aggregation of the whole substrate may generate more SERS hotspots, which are crucial for the electromagnetic enhancement of SERS signals. In one word, the three-layer structure of the composite material has been successfully designed.

In order to better analyze the composite of GO and Au NPs, the comparison of the Raman spectrum for GO and Fe_3O_4/GO/Au was shown in Fig. 4. The peak intensity of Fe_3O_4/GO/Au is obviously higher than GO. It demonstrated that Au NPs have a high SERS enhancement effect for GO. The two groups of Raman spectra can clearly display the

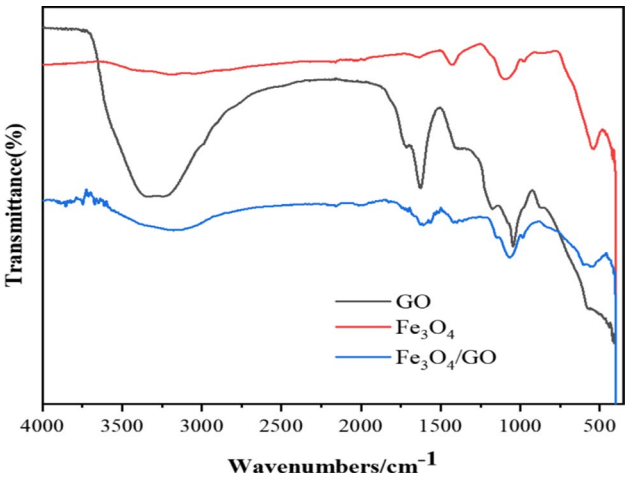

Fig. 2 Infrared spectra of the GO, Fe_3O_4, and Fe_3O_4/GO/Au

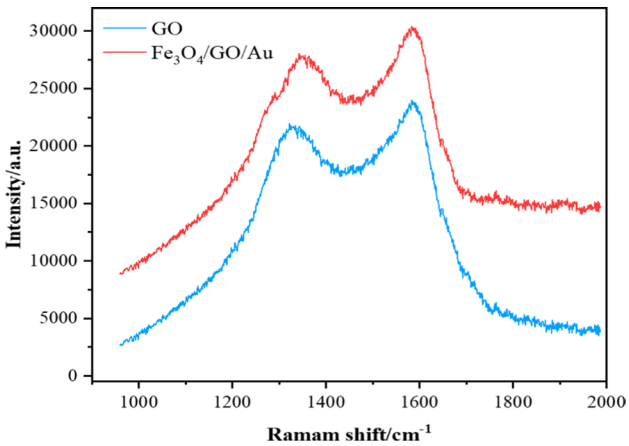

Fig.4 Raman spectra of GO and Fe_3O_4/GO/Au

characteristic peaks of GO, that is, the D peak (close to 1350cm^{-1}) corresponds to the defective carbon bond structure, which is related to the vibration of sp^3 carbon atoms. The G peak located at 1583cm^{-1} corresponds to the E_{2g} vibrational mode structure of graphite SP^2 carbon atom phonons (Tene et al. 2023). The Raman signal of Fe_3O_4/GO/Au nanocomposites is stronger than that of graphene oxide materials, indicating that the prepared Au NPs have a strong surface-enhanced Raman spectroscopic effect based on SPR.

TEM image of Fe_3O_4/GO/Au NPs is presented in Fig. 5a. As seen in Fig. 5, the prepared Fe_3O_4 NPs are dark gray with agglomeration. The black dots are Au with a particle size of less than 50 nm and uniform distribution. The slightly wrinkled thin layer is GO. It is shown that Au and Fe_3O_4 NPs are effectively adsorbed on the GO. It is confirmed that Fe_3O_4/GO/Au is successfully prepared (Liu et al. 2022a, b). The EDSX of the Fe_3O_4/GO/Au NPs is presented in Fig. 5b. The Fe, O, and Au elements were accurately identified.

SERS performance

10^{-6} M of R6G was selected as a Raman probe. From Fig. 6, it can be seen that the Raman signal of R6G with Au NPs as substrate was weak. However, SERS spectra of R6G with a high signal-to-noise ratio were obtained with Fe_3O_4/GO/Au nanocomposite material as the substrate. Among them, the C=C double bond stretching vibration characteristic spectra (1312, 1345, and 1566 cm^{-1}) and in-plane and out-of-plane deformation vibration characteristic spectra (610, 774, and 1182 cm^{-1}) related to the benzene ring of R6G molecule were significantly enhanced (Seo and Ha 2018). The above results demonstrate that Fe_3O_4/GO/Au composite materials enhance the SERS of R6G. It may be attributed to the adsorbability of graphene and the SPR of Au NPs so that it reduced the distance between the substrate and the probe molecules. As a result, the SERS signal of R6G improved remarkably. Therefore, the prepared Fe_3O_4/GO/Au composite material can serve as an active SERS substrate for rapid detection.

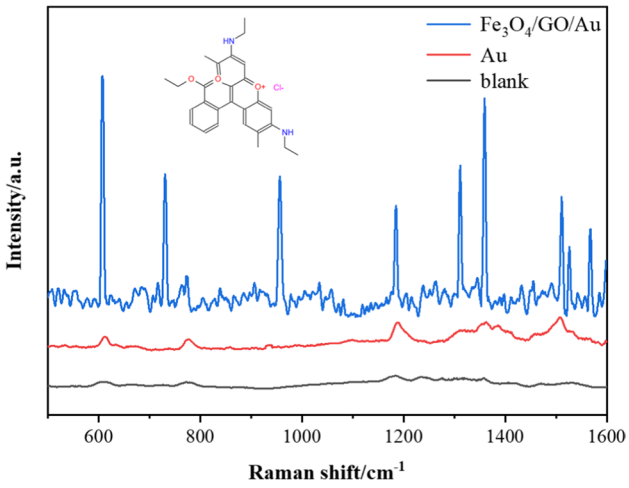

Fig. 6 The Raman spectra of R6G from Au and Fe_3O_4/GO/Au

SERS detection of mancozeb

The obtained Fe_3O_4/GO/Au composite material was used as SERS active substrate, Raman spectra of different concentrations of mancozeb in pyridine solution were collected, and the spectra of pyridine were given as control. Figure 7 shows the average spectrum of mancozeb in the range of 0.125–25 ppm (0.125 ppm, 0.25 ppm, 1.25 ppm, 2.5 ppm, 12.5 ppm, and 25 ppm), and all spectra are smoothed. The strong band at 665 cm^{-1} can be attributed to the interaction between Zn and Mn and C-S–S groups, the strong band at 953 cm^{-1} may correspond to the stretching vibration of C-S. The weak

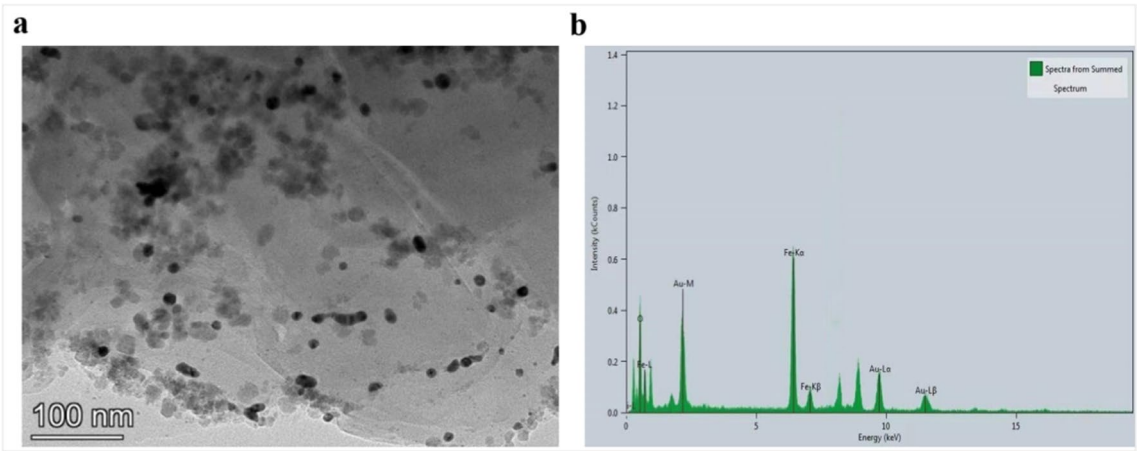

Fig. 5 TEM imaging of Fe_3O_4/GO/Au microspheres (**a**) and EDX (**b**)

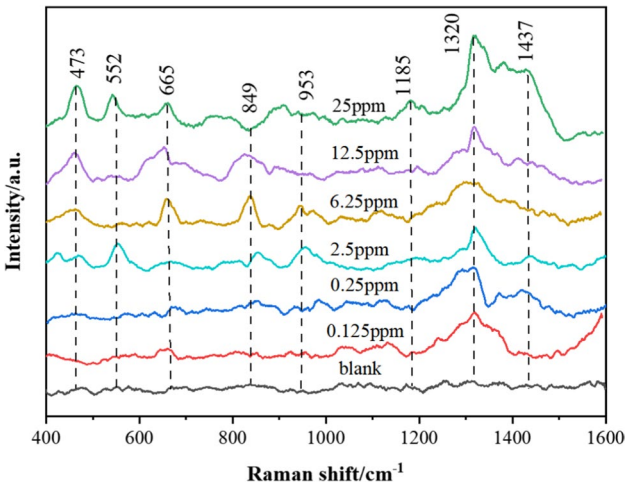

Fig. 7 Raman spectra of different concentrations of mancozeb

band at 849 cm^{-1} can be attributed to the bending vibration of N–H. The vibration at 1185 cm^{-1} can be attributed to the coupling of CH_3 rotational vibration and C-N stretching vibration, and the detected spectral band at 1320 cm^{-1} may be caused by the coupling of N–H and C–C stretching vibration (Tsen et al. 2021).

In order to quantitatively analyze mancozeb, we plotted a working curve using the intensity of mancozeb at 1320 $cm^{-1}$with different concentrations. It can be seen that the intensity of SERS increases with the increase of mancozeb concentration. As shown in Fig. 8, the standard curve showed perfect linearity in the range of 0.25 ~ 25 ppm (0.25 ppm, 1.25 ppm, 2.5 ppm, 12.5 ppm, and 25 ppm), with the correlation coefficient R^2 of 0.9927, and the optimal fitting equation was $Y = 1057.7X + 7954$. These results indicate

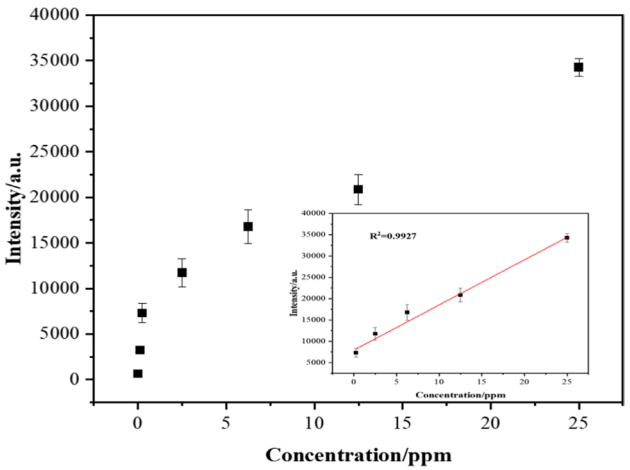

Fig. 8 The corresponding calibration plot of Raman intensity versus the concentrations of mancozeb

that Fe_3O_4/GO/Au composite materials as SERS active substrates can meet the requirements of quantitative detection.

Determination of mancozeb in pakchoi

In order to evaluate the feasibility of the developed method for application, the real sample as a representative, pakchoi purchased from the supermarket was detected. To minimize the influence of the pakchoi matrix, the QuEchERS method was employed for extraction. The results proved that the mancozeb was undetected in pakchoi. Subsequently, three different concentrations of mancozeb were artificially added to the unprocessed pakchoi for recovery. As shown in Table 1, the developed SERS method exhibited recovery ranging from 82.0 to 102% for detecting mancozeb in pakchoi and water. The recovery of water is better than pakchoi. Maybe it is attributed to the loss of mancozeb in the process of extraction.

Activity, stability, and repeatability of Fe_3O_4/GO/Au

In order to quantify the SERS ability, the analytical enhancement factor (EF) was estimated, using the following equation: $EF = I_{SERS} \times C_0 / I_0 \times C_{SERS}$, where I_{SERS} and I_0 are the intensity of SERS and the normal Raman (Bell et al 2020). The C_{SERS} and C_0 are the concentrations of mancozeb absorbed at Fe_3O_4/GO/Au (0.125 ppm) and on bare mancozeb (25 ppm). The EF for the mancozeb at 1320 cm^{-1} was 3.28×10^4. This may be attributed to the contribution of two different enhancement mechanisms, namely, electromagnetic enhancement and chemical enhancement. The formulation (LOD = 3δ/k) was used to determine the limit of detection (LOD), where δ represents the standard deviation of intensities from the blank platform and k is the slope of the calibration curve. At peak 1320 cm^{-1}, the calculated LOD was 0.077 ppm. The aforementioned SERS experiment confirms that Fe_3O_4/GO/Au has a greater capacity to identify mancozeb. The comparison of different materials for mancozeb detection is listed in Table 2.

Stability is a critical feature for any outstanding SERS-active substrate in practical application. To examine the stability of Fe_3O_4/GO/Au, time-dependent SERS measurements

Table 1 Results of recovery experiments for detecting mancozeb

Samples	Spiked (ppm)	Detected (ppm)	Recovery (%)
Pakchoi	0.50	0.41 ± 0.08	82
	1.00	0.88 ± 0.05	88
	3.00	2.66 ± 0.06	89
River water	0.50	0.48 ± 0.07	96
	1.00	1.02 ± 0.03	102
	3.00	2.91 + 0.08	97

Table 2 The comparison of different materials for mancozeb detection

Analyte	Material	Detection concentration	References
Mancozeb	Silver colloids	0.3 ppm	Cortes (1998)
Mancozeb	Au and Ag NSs	2.8×10^{-3} M	Atanasov et al. (2019a, b)
Mancozeb	Ag@Au	0.2 ppm	Tsen et al. (2021)
Colorants	GO/Au@Ag	10^{-9} mol/L	Kong et al. (2021)
Glucose	GO/Au@Ag	0.4728 mol/L	Song et al. (2018)
Clenbuterol	GO/Au	3.34×10^{-8} mol/L	Sun et al. (2020)
Patulin	GO/Au	0.46 ng/mL	Xue et al. (2024)
Rhodamine B	Fe_3O_4/GO/Au	10^{-8} mol/L	Xu et al. (2019)
Phenanthrene	Fe_3O_4/GO/Au	5.6×10^{-10} mol/L	Liu et al. (2022a, b)
Bifenthrin	Fe_3O_4/GO/Au	10^{-8} mol/L	Song et al. (2023)
Mancozeb	Fe_3O_4/GO/Au	0.07 ppm	Wu et al. (this work)

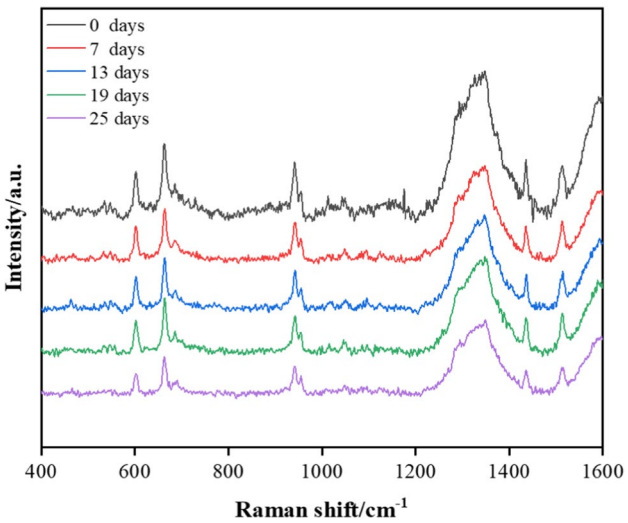

Fig. 9 SERS spectra of 25 ppm mancozeb on storage samples with various periods

were performed, as shown in Fig. 9. It showed that the intensity of the SERS signal did not obviously change over 25 days. It indicated that the Fe_3O_4/GO/Au substrate is stable during preservation.

In addition, the repeatability of Raman signals is an important factor for the performance of SERS substrate. To assess the repeatability of Fe_3O_4/GO/Au, three samples were obtained following the same conditions, at 11 random locations on the substrate. The results clearly show that the Fe_3O_4/GO/Au as SERS substrate has high repeatability, with a low RSD of approximately 4.4% (Fig. 10).

Mechanism exploration

Generally, it contains an electromagnetic enhancement mechanism (EM) and chemical reinforcement mechanism (CM) for SERS(Jensen et al 2008; Cialla et al 2012; Valley et al 2010; Morton, et al 2009). For our research, the

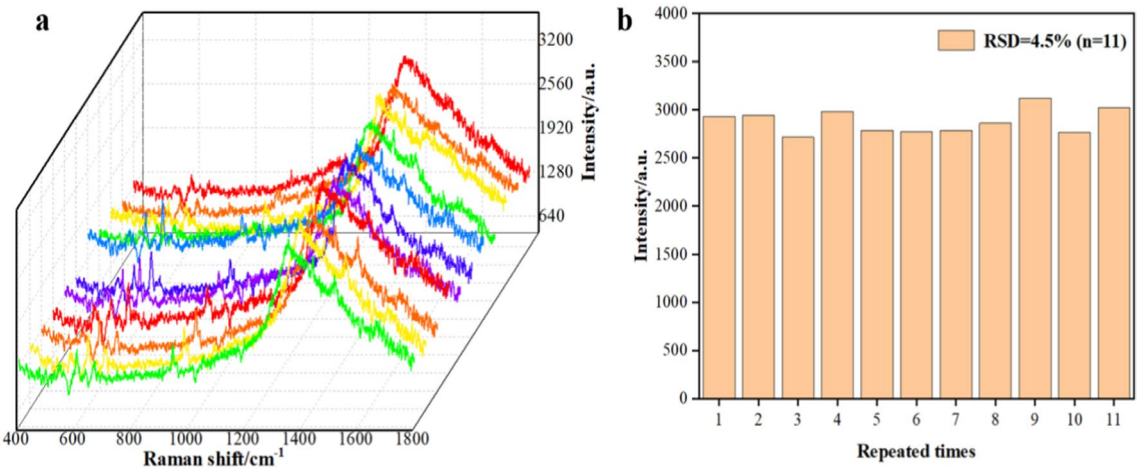

Fig. 10 **a** SERS spectra of mancozeb from 11 randomly selected substrates. **b** The Raman intensity distribution of 1320 cm^{-1} peak from the obtained 11 spectra

Au in the Fe_3O_4/GO/Au substrate plays a significant role in enhancement because of LSPR and the coordination between Au and mancozeb molecular with sulfhydryl and amino group. Due to the coordination interaction, the distance between the substrate and target molecule gets shorter, in the region of the hot spot or junction. In addition, because of the adsorption property of GO, maybe it adsorbs target molecules and shortens the distance between them. Furthermore, maybe there is a coupling effect between transition metal (Fe) and noble metal nanostructures (Au) which improve the reflectivity of incident light. As a result, the local electromagnetic field intensity near the noble metal nanostructure strengthened. Furthermore, the magnetic properties of the Fe_3O_4 create a high density of interparticle hot spots by magnetism-induced aggregation which endow the Fe_3O_4 with enrichment ability. Due to the abovementioned reason, the substrate and target molecule get closer and closer. As a result, the electromagnetic field will be enhanced in the region of the hot spot, and the Raman signal will be amplified.

Chemical reinforcement mechanism mainly includes ground state chemical enhancement mechanism, resonance Raman enhancement mechanism, and charge transfer (CT) enhancement mechanism (Zhang, et al 2022). The mechanism of CT enhancement means that when the target molecules are adsorbed on the surface of precious metal nanoparticles, chemical bonds are formed. When incident light irradiates on the surface of noble metal nanoparticles and the energy of incident light match that of the charge transfer, also if the Fermi energy level of the metal surface is between the lowest unoccupied molecular orbital (LUMO) and the highest occupied molecular orbital (HOMO) of the adsorbed molecule, resonance Raman scattering occurs. The free electrons on the surface of the metal will resonate and transit to the adsorbed molecule. The process of resonant electron transition will increase the polarizability of adsorbed molecules. Thus, the Raman signal of adsorbed molecules is enhanced. Meanwhile, due to the tunable band gap, semiconductors have attracted researchers' attention in the SERS application. Because of the distinctive charge transfer capability, semiconductors have the possibility to match the energy levels of target molecules with large SERS enhancement (Zhang et al 2021). The CT route was found to be the excitation of electrons from the conduction bands of the semiconductor to the LUMO of the molecule. For our research, maybe the free electrons resonate and transit from the conduction band of GO and excited states of Au NPs to LUMO mancozeb, as shown in Fig. 11. Initially, the energy gap between the HOMO and LUMO can witness the direct resonant Raman scattering by laser. The excess of electrons can be contributed from GO and Au NPs, which endow the Raman signals further enhancement by the EM and CM (Ye et al 2012; Mandavkar et al 2022; Rajput et al. 2022).

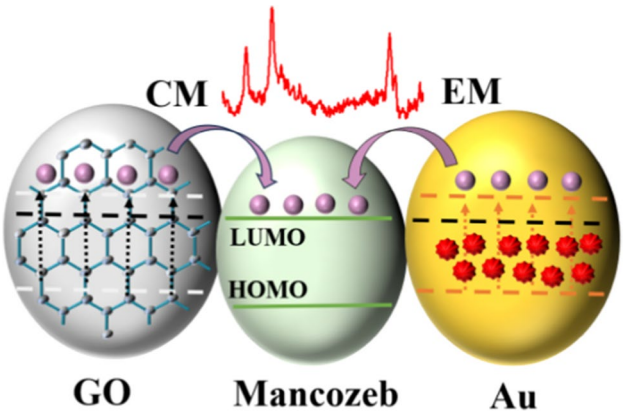

Fig. 11 Schematic of CM and EM enhancements in the SERS process

Conclusion

In the study, a three-layer multifunctional Fe_3O_4/GO/Au composite nanomaterial with a high hot spot was designed and prepared as a reinforced matrix. This composite material enabled the rapid, sensitive, and quantitative detection of mancozeb using the SERS method. The magnetic precious metal composite nanomaterials were characterized and analyzed. The Fe_3O_4/GO/Au and Au NPs were experimentally investigated using R6G as the probing molecule. The results demonstrated that the prepared composite nanomaterials exhibited excellent performance than single Au NPs for SERS assay. Moreover, the Fe_3O_4/GO/Au composite was successfully applied to detect mancozeb, showing linear correlations ranging from 0.25 to 25 ppm at 1320 cm^{-1}. The linear relationship was represented by the equation $Y = 1057.7X + 7954$, with a coefficient of determination (R^2) of 0.9927. When applied to actual samples, the method exhibited acceptable recoveries, indicating excellent accuracy and applicability for detecting mancozeb in pakchoi. The proposed method showed well sensitivity to mancozeb with a limit of detection (0.077 ppm) and high EF, stability, and repeatability. In addition, the mechanism of SERS enhancement with EM and CM was discussed in detail, which provides a new perspective in understanding SERS mechanisms. The main advantages of this method are short sample pretreatment time with multi-function and strong signal amplification. It is expected to achieve quantitative detection of pesticide residues in the fields of food, agriculture, and the environment.

Authors contribution Rui Wu: conceptualization, funding acquisition, investigation, resources, project administration. Xi Song: writing original, data curation, validation, draft methodology, review, editing, supervision. Guanghui Tian: formal analysis.

Funding This work was supported by the Natural Science Foundation of Shaanxi Province (2024GX-YBXM-318, 2023-YBGY-486, 2022SF-356), the Education Research Project of Shaanxi University of Technology (JYYJ2023-16), and the National Natural Science Foundation of China (22177066).

Data availability All data included in this study are available upon request by contact with the corresponding author.

Declarations

Ethics approval This study does not involve animal experiments or human participants, and there is no ethical problem.

Consent to participate All the authors consent to participate in this article.

Consent for publication All the authors consent to publish this article.

Competing interests The authors declare no competing interests.

References

Akamine LA, Medina DAV, Lanças FM (2021) Magnetic solid-phase extraction of gingerols in ginger containing products. Talanta 222:121683–121692

Atanasov PA, Nedyalkov NN, Fukata N, Jevasuwan W, Subramani T, Hirsch D, Rauschenbach B (2019a) Au and Ag films and nanostructures for detection of fungicide mancozeb: SERS analyses. AIP Conf Proc 2075:030001

Atanasov PA, Nedyalkov NN, Fukata N, Jevasuwan W, Subramani T, Terakawa M, Nakajima Y (2019b) Surface-enhanced Raman spectroscopy (SERS) of mancozeb and thiamethoxam assisted by gold and silvernanostructures produced by laser techniques on paper. Appl Spectrosc 73:313–319

Avadaiappan A, Antony SJ, Franci B, Mahalingam U, Ramasamy P, Conchalish H, Sath V (2022) Environmental photochemistry with thiol- and silica-modified plasmonic nanocomposites: SERS sensing of municipal solid waste and tannery waste leachate from groundwater. Environ Sci Pollut Res 29:90023–90033

Bell S, Charron G, Cortés E, Kneipp J (2020) Towards reliable and quantitative surface-enhanced Raman scattering (SERS): from key parameters to good analytical practice. Angew Chem Int Edit 59:5454–5462

Bi C, Wang Z, Zhao H, Liu G (2023) Facile synthesis of multibranched gold nanostars with precisely tunable sizes for surface-enhanced Raman scattering. J Mater Chem C 11:10333–10340

Cialla D, März A, Böhme R (2012) Surface-enhanced Raman spectroscopy (SERS): progress and trends. Anal Bioanal Chem 403:27–54

Cortes S S, Vasina M, Francioso O, Garcıa RJV (1998) Raman and surface-enhanced Raman spectroscopy of dithiocarbamate fungicides. Vib Spectrosc 17:133–144

Dall'Agnol JC, Pezzini MF, Uribe NS, Joveleviths D (2021) Systemic effects of the pesticide mancozeb-aliterature review. Eur Rev Med Pharmaco 25:4113–4120

Deng X, Wang S, Zhou W, Xu M, Chen B, Zhang W (2023) Wrinkle-bioinspired silver nanowire surfaceenhanced Raman scattering sensors for pesticide molecule detection. Anal Bioanal Chem 415:1–10

Dick S, Konrad MP, Lee WW, McCabe H, McCracken JN, Rahman TM, Bell SE (2016) Surface-enhanced Raman spectroscopy as a probe of the surface chemistry of nanostructured materials. Adv Mater 28:5705–5711

Fu XL, Wu HY, Liu ZH, Wang PZ (2024) MoS_2 nanosheets as substrates for SERS-based sensing.ACS Appl. Nano Mater 7:3988–3996

Ghanei M, Hosseinifar A (2020) A novel amperometric hydrogen peroxide sensor based on gold nanoparticles supported on Fe_3O_4@polyethyleneimine. Int J Environ an Ch 100:591–601

Han XX, Rodriguez RS, Haynes CL, Ozaki Y, Zhao B (2021) Surface-enhanced raman spectroscopy. Null 1:87–91

He J, Song G, Wang X, Zhou L, Li J (2022) Multifunctional magnetic Fe_3O_4/GO/Ag composite microspheres for SERS detection and catalytic degradation of methylene blue and ciprofloxacin. J Alloy Compd 893:162226–162235

Jensen L, Aikens CM, Schatz GC (2008) Electronic structure methods for studying surface-enhanced Raman scattering. Chem Soc Rev 37(5):1061–1073

Ji S, Zhang F, Yao P et al (2023) Optimization of pig manure-derived biochar for ammonium and phosphate simultaneous recovery from livestock wastewater. Environ Sci Pollut Res 30:82532–82546

Jing Y, Yuan X, Yuan Q, He K, Liu Y, Lu P, Li G (2016) Determination of nicotine in tobacco products based on mussel-inspired reduced graphene oxide-supported gold nanoparticles. Sci Rep-Uk 6:29230–29237

Jinzi Y, Chunyan Z (2020) Preparation of magnetic Fe_3O_4 nanoparticles. Fine Chem Intermed 50:50–53

Khan MF, Jamal A, Rosy PJ, Alguno AC, Ismail M, Khan I, Zahid M (2022) Eco-friendly elimination of organic pollutants from water using graphene oxide assimilated magnetic nanoparticles adsorbent. Inorg Chem Commun 139:109422–109432

Kong LL, Chen J, Huang MZ (2021) GO/Au@Ag nanobones decorated membrane for simultaneous enrichment and on-site SERS detection of colorants in beverages. Sensor Actuat B-Chem 344:130163–130171

Lin Y, Ding D, Hu C, Li Z, Shen Y, Xia F (2021) The differences of graphene oxide products made from three kinds of flake graphites. ACS Omega 6:25996–26003

Liu J, Liu Y, Cao Y, Sang S, Guan L, Wang Y, Wang J (2022a) Preparation of Fe_3O_4@PDA@Au@GO composite as SERS substrate and its application in the enrichment and detection for phenanthrene. Micromachines-Basel 13:128–141

Liu JY, Liu YW, Cao YD, Sang SH, Guan L (2022b) Preparation of Fe_3O_4@PDA@Au@GO Composite as SERS substrate and its application in the enrichment and detection for phenanthrene. Micomachines 13:128–142

Liu YH, Dang A, Liu X, Han YY, Chen JH, Zada A, Sun YT, Yuan ZQ, Luo F, Li TH, Zhao TK (2024) Synergistic resonances and charge transfer in double-shelled ZnO hollow microspheres for high-performance semiconductor-based SERS substrates. ACS Appl Nano Mater 7:10104–10113

Łozowicka B, Rutkowska E, Jankowska M (2017) Influence of QuEChERS modifications on recovery and matrix effect during the multiresidue pesticide analysis in soil by GC/MS/MS and GC/ECD/NPD. Environ Sci Pollut Res 24:7124–7138

Mandavkar R, Lin S, Pandit S (2022) Hybrid SERS platform by adapting both chemical mechanism and electromagnetic mechanism enhancements: SERS of 4-ATP and CV by the mixture with GQDs on hybrid PdAg NPs. Surf Interfaces 33:102175–102189

Meenakshi MM, Annasamy G, Sankaranarayanan M (2023) Highly sensitive technique for detection of adulterants in centella herbal samples using surface enhanced Raman spectroscopy (SERS). SpectrochimActa A 299:122878–122889

Morton SM, Ewusi AE, Jensen L (2009) Controlling the non-resonant chemical mechanism of SERS using a molecular photoswitch. Phys Chem Chem Phys 11:7424–7429

Pan TT, Guo W, Lu P, Hu D (2021) In situ and rapid determination of acetamiprid residue on cabbage leaf using surface-enhanced Raman scattering. J Sci Food Agr 101:3595–3604

Rajput SV, Guptab RK, Prakash J (2022) Engineering metal oxide semiconductor nanostructures for enhanced charge transfer: fundamentals and emerging SERS applications. J Mater Chem C 10:73–95

Sakano T, Tanaka Y, Nishimura R, Nedyalkov NN, Atanasov PA, Saiki T, Obara M (2008) Surface enhanced Raman scattering properties using Au-coated ZnO nanorods grown by two-step, off-axis pulsed laser deposition. J Phys d: Appl Phys 41:235304–235310

Seo M, Ha JW (2018) Effective surface-enhanced Raman scattering of randomly branched gold nano-urchins with Rhodamine 6G as Raman reporters. Microchem J 140:47–51

Shukla SK, Gupta R, Gupta RK, Prakash J (2023) Highly efficient visible light active doped metal oxide photocatalyst and SERS substrate for water treatment. Environ Sci Pollut Res 30:34054–34068

Song DD, Zhou YYY, Liu Y, Song SS (2018) Hybrid hydrogels based on insitu interpenetrating networks graphene oxide (GO) and Au nanoparticles, and its application as peroxidase mimetics for glucose detection. Chem Select 3:10259–10264

Song Y, Xiao KY, Chen Q, Zhang XD, Yu Z (2023) Fabrication of GO/Fe_3O_4@Au MNPs for magnetically enriched and adsorptive SERS detection of bifenthrin. Chemosensors 11:4832–4840

Sun Y, Chen H, Ma P, Li JY, Zhang Z, Shi H (2020) In situ synthesis of graphene oxide/gold nanocomposites as ultrasensitive surface-enhanced Raman scattering substrates for clenbuterol detection. Anal Bioanal Chem 412:193–201

Supriyanto G, Rukman NK, Nisa AK, Jannatin M (2018) Graphene oxide from Indonesian biomass: synthesis and characterization. Bioresources 13:4832–4840

Suzuki S (2019) Synthesis of graphene-based materials for surface-enhanced Raman scattering applications. E-J Surf Sci Nanotec 17:71–82

Tene T, Guevara M, Palacios FB, Barrionuevo TPM, Gomez CV, Bellucci S (2023) Optical properties ofgraphene oxide. Front Chem 11:1–14

Tiryaki E, Zorlu T, Puebla RA (2024) Magnetic-plasmonic nanocomposites as versatile substrates for surface-enhanced Raman Scattering (SERS) Spectroscopy. Chem Eur J 30:03987–04000

Tsen CM, Yu CW, Chen SY, Lin CL, Chuang CY (2021) Application of surface-enhanced Raman scattering in rapid detection of dithiocarbamate pesticide residues in foods. Appl Surf Sci 558:149740–149751

Valley N, Jensen L, Autschbach J, Schatz GC (2010) Theoretical studies of surface enhanced hyper-Raman spectroscopy: the chemical enhancement mechanism. J Chem Phys 133(5):054103–054110

Van Vu S, Nguyen AT, Tran ATC, Le VHT, Lo TNH, Ho TH, Vo KQ (2023) Differences between surfactant-free Au@ Ag and CTAB-stabilized Au@ Ag star-like nanoparticles in the preparation of nanoarrays to improve their surface-enhanced Raman scattering (SERS) performance. Nanoscale Adv 5:5543–5561

Wang Z, Yang L, Ye X, Huang C, Yang W, Zhang L, Fu F (2020) Multicolor visual screening of totaldithiocarbamate pesticides in foods based on sulfydryl-mediated growth of gold nanobipyramids. Anal-Chim Acta 1139:59–67

Wang Y, Meng Z, Su C, Fan S, Li Y, Liu H, Li Q (2022) Rapid screening of 352 pesticide residues inchrysanthemum flower by gas chromatography coupled to quadrupole-orbitrap mass spectrometry withSin-QuEChERS nanocolumn extraction. J Anal Methods Chem 2022:7684432–7684449

Weis JE, Vejpravova J, Verhagen T, Melnikova Z, Costa S, Kalbac M (2018) Surface-enhanced Raman spectra on graphene. J Raman Spectrosc 49:168–173

Weng S, Zhu W, Dong R, Zheng L, Wang F (2019) Rapid detection of pesticide residues in paddy water using surface-enhanced Raman spectroscopy. Sensors-Basel 19:506–516

Wu H, Luo Y, Hou C, Huo D, Wang W, Zhao J, Lei Y (2019) Rapid and fingerprinted monitoring of pesticide methyl parathion on the surface of fruits/leaves as well as in surface water enabled by goldnanorods based casting-and-sensing SERS platform. Talanta 200:84–90

Wu R, Song J, Lu JF, Ji XH, Tian GH, Zhang F (2023) Constructions of Fe_3O_4/HAp/Au nanohybrids with multifunctional structure for efficient photocatalysis and environmental remediation of organic dyes. J Mol Struc 1278:134908–134914

Xu LL, Suo HB, Wang JL, Cheng FX, Liu HM (2019) Magnetic graphene oxide decorated with chitosan and Au nanoparticles: synthesis, characterization and application for detection of trace rhodamine B. Anal Methods 30:3837–3843

Xu L, Abd El-Aty AM, Eun JB, Shim JH, Zhao J, Lei X, Hammock BD (2022a) Recent advances in rapid detection techniques for pesticide residue: a review. J Agr Food Chem 70:13093–13117

Xu L, Zhang X, Abd El-Aty AM, Wang Y, Cao Z, Jia H, Hammock BD (2022b) A highly sensitive bio-barcode immunoassay for multi-residue detection of organophosphate pesticides based on fluorescenceanti-quenching. J Pharm Anal 12:637–644

Yang L, Hu G, Huang Y, Wang C, Liu X, Lu C, Ma G (2022) Simple and sensitive determination of sulfites in Chinese herbal teas by ultrahigh-performance liquid chromatography tandem mass spectromety. Anal Methods-Uk 14:2849–2856

Yang Q, Sun DW, Pu H (2023) Porous materials nanohybridized with metal nanoparticles as substrates for enhancing SERS detection in food safety applications. Trends Food Sci Tech 16:104202–104216

Ye Y, Hutchison JA, Uji H, Hofkens J (2012) Excitation wavelength dependent surface enhanced Raman scattering of 4-aminothiophenol on gold nanorings. Nanoscale 4:1606–1611

Ye M, Beach J, Martin JW, Senthilselvan A (2017) Pesticide exposures and respiratory health in generalpopulations. J Environ Sci 51:361–370

Ye P, Xin W, De Rosa IM, Wang Y, Goorsky MS, Zheng L, Xie YH (2020) One-pot self-templated growth of gold nanoframes for enhanced surface-enhanced Raman scattering performance. Acs Appl Mater Inter 12:22050–22057

Ying Y, Tang Z, Liu Y (2023) Material design, development, and trend for surface-enhanced Raman scattering substrates. Nanoscale 15:10860–10881

Zhang M, Wang YN, Wang X, Zhao B, Ruan WD (2021) Surface-enhanced Raman Scattering (SERS) on indium-doped CdO (ICO) substrates: a new charge-transfer enhancement contribution from electrons in conduction bands. J Phys Chem C 125:17125–17132

Zhang J, Xing TY, Zhang M (2022) Facile preparation of Cu_2-xS supernanoparticles with an unambiguous SERS enhancement mechanism. Chem Eng J 434:134457–134464

Zheng X, Zhang W, Zhang J, Wang L (2021) Synthesis of yolk-shell Fe_3O_4@void@CeO_2 nanoparticles and their application in SERS. Appl Surf Sci 541:148422–148428

Zheng ZJ, Xu K, Lu FF, Zhong B, You LJ (2023) Magnetic covalent organic framework for the adsorption of silver nanoparticles and recycled as surface-enhanced Raman substrate and high-efficiency catalysts for 4-nitrophenol degradation. Environ Sci Pollut Res 30:34636–34648

Zhou H, Li X, Wang L, Liang Y, Jialading A, Wang Z, Zhang J (2021) Application of SERS quantitative analysis method in food safety detection. Rev Anal Chem 40:173–186